Determination of population, alignment, and orientation using laser induced fluorescence with unresolved emission

Andrew C. Kummel, Greg O. Sitz, and Richard N. Zare
Department of Chemistry, Stanford University, Stanford, California 94305

(Received 5 February 1988; accepted 9 March 1988)

A method is presented for determining the population, $A_{0+}^{\{0\}}$, the alignment moments, $A_{q\pm}^{\{2\}}$ and $A_{q\pm}^{\{4\}}$, and the orientaion moments, $A_{q\pm}^{\{1\}}$ and $A_{q\pm}^{\{3\}}$, for a ground state distribution of diatomic molecules probed by 1 + 1 laser induced fluorescence. General expresssions are developed for all rotational branches as a function of the rotational quantum number for excitation with linearly, circularly, or elliptically polarized light. Specific expressions are evaluated for the case in which the emission is unresolved and collected independent of its polarization and for the case in which the emission is unresolved but is analyzed with a polarizer. When the emission is collected independent of its polarization, the *real* polarization moments, $A_{q\pm}^{\{k\}}$, cannot be independently determined and only the apparent moments, $A_{q\pm}^{\{k\}}$ (app), can be measured, explicit expressions for the apparent moments in terms of the real moments are presented. However, for the case in which the excitation light is created by passing linearly polarized light through a quarter-wave plate and the emitted light is analyzed with a quarter-wave plate and a linear polarizer, the real alignment and orientation moments can be independently determined.

I. INTRODUCTION

This paper presents the theory required to determine the population, alignment, and orientation of an ensemble of molecules using 1 + 1 laser induced fluorescence (LIF) (one photon absorbed and one photon emitted). The alignment locates the molecular plane of rotation, while the orientation describes the net helicity of the angular momentum vector **J**. In the $|JM\rangle$ representation, the alignment is determined by the probability of the molecule being in sublevels M or $-M$ as opposed to sublevels M' or $-M'$. Orientation implies that the molecule has a greater probability of being in sublevel M as opposed to sublevel $-M$. Thus, alignment refers to the even moments of the M distribution, orientation to the odd moments.

This paper treats the most general case: detection of population, alignment, and orientation with LIF in which both the absorption and emission are polarization analyzed and resolved. This can be achieved by passing narrow bandwidth, linearly polarized laser light through a quarter-wave plate and analyzing the emitted light with a quarter-wave plate, a linear polarizer (such as a calcite prism or a sheet polarizer), and a monochromator. When employing a single experimental geometry, elliptically polarized light is required to determine independently the multiple orientation moments and polarized detection is required to determine independently the multiple alignment moments.

Experimentally, analyzing the fluorescence with a quarter-wave plate, a polarizer, and a monochromator is very difficult. Consequently, we also treat the more common case in which the probe light is polarized but the fluorescence is collected independently of both its wavelength and polarization. Removal of the monochromator reduces the number of orientation moments that we measure independently, but removal of the quarter-wave plate and the polarization analyzer greatly affects our ability to measure the real polarization moments, $A_{q\pm}^{\{k\}}$. Without polarization analysis of the fluorescence, we can only measure the apparent moments, $A_{q\pm}^{\{k\}}$ (app), which are known combinations of a greater number of real moments, $A_{q\pm}^{\{k\}}$.

There are two important excitation–detection geometries (see Fig. 1): In case I, *the coaxial geometry*, the excitation light propagates along the $-z$ axis and the detector is situated along the y axis. In case II, *the mutually orthogonal geometry*, the laser propagates along the $-x$ axis, while the detector is situated along the y axis. These two geometries measure different moments. For a system with near-cylindrical symmetry, the axis of near-cylindrical symmetry is always designated as the z axis, and case I geometry is useful for measuring the orientation about z, ($A_{0+}^{\{1\}}$), and for sensing the alignment in the x–y plane, ($A_{2+}^{\{2\}}$). However, case II geometry is very sensitive to the alignment about the z axis, ($A_{0+}^{\{2\}}$). We present the results for these two cases, but we give the general formulas for any excitation–detection geometry as well as specific formulas for excitation and detection along the $-z$, $-x$, and y axes, called cases A, B, and C, respectively.

The formulas in this paper are a direct extension of those in our previous papers[1,2] (hereafter denoted as KSZ1 and KSZ2) for determining the population, orientation, and alignment of the ground state using two-photon nonresonant excitation with elliptically polarized light. The techniques developed in these papers are applicable to atoms, diatomics molecules, and symmetric top polyatomic molcules; generalization to asymmetric top molecules is straightforward. Several groups[3–6] have worked on developing the formalism required to measure the population and polarization of the ground state using LIF. The most relevant work may be that of Bain and McCaffery.[6] They clear-

 0021-9606/88/127357-12$02.10

ly showed that with a fixed excitation–detection geometry one cannot independently measure the multiple orientation moments when using circularly and linearly polarized excitation of a single rotational line. They also showed that multiple alignment moments cannot be determined by using linearly polarized excitation and restricting oneself either to varying the polarization of the excitation light or to analyzing the polarization of the fluroescence from a single rotation line. Bain and McCaffery[6] assume that the fluorescence is wavelength resolved. None of the previous work[3–6] considers the additional information that can be obtained when using elliptically polarized light, multiple rotational branches (except Dixon[5]), or covariation of excitation polarization and fluorescence polarization analysis. It is these three techniques which allow us to overcome the problems identified by Bain and McCaffery.[6]

II. ABSORPTION PROBABILITY FOR ELLIPTICALLY POLARIZED LIGHT

The only difference between calculating the two-photon nonresonant absorption probability and the 1 + 1 LIF intensity is that in the former case the first photon excites the molecule to a virtual state, while in the latter case the first photon places the molecule in a real state. Consequently, we can readily convert the equations in Table II of KSZ2 for use in LIF by removing the sums over the quantum numbers of the excited state and adding a term for depolarization of the excited state. Consequently, for a molecule excited from the ground state (J_i,Λ_i) to the excited state (J_e,Λ_e) and fluorescing back down to the final state (J_f,Λ_f), we write

$$I = C(\det) n(J_i) \sum_{k,q,J_f} \times \left[P_{q+}^{\{k\}}(J_i,\Lambda_i,J_e,\Lambda_e,J_f,\Lambda_f;\Omega) A_{q+}^{\{k\}}(J_i) + P_{q-}^{\{k\}}(J_i,\Lambda_i,J_e,\Lambda_e,J_f,\Lambda_f;\Omega) A_{q-}^{\{k\}}(J_i) \right], \quad (1)$$

where

$$P_{q\pm}^{\{k\}}(J_i,\Lambda_i,J_e,\Lambda_e,J_f,\Lambda_f;\Omega) = b^k(J_i) g^k(J_i) g^k(J_e) \sum_{k_d,k_a} \times (-1)^{(k)} \epsilon_{q\pm}^{\{k\}}(k_d,k_a;\Omega_{\rm lab}) \times S(J_i,\Lambda_i,J_e,\Lambda_e,J_f,\Lambda_f) h(k_d,k_a,k,J_i,J_e,J_f) \quad (2)$$

and $k = 0,1,2,3,4$; $q = 0,1,2,3,4$ but $q \leqslant k$; $k_d = 0,1,2$; $k_a = 0,1,2$. The terms in Eqs. (1) and (2) are as follows: $C(\det)$ is the detection sensitivity constant; $n(J_i)$ is the rotational population in the ground electronic state; $P_{q\pm}^{\{k\}}$ are the moments of the line strength; $A_{q\pm}^{\{k\}}$ are the moments of the ground state angular momentum distribution for level J_i (see Sec. IV of KSZ2); $b^k(J_i)$ are the reduced matrix elements of the spherical tensor angular momentum operators; $g^k(J_i)$ and $g^k(J_e)$ are the hyperfine and spin depolarization factors for the ground and excited states; $\epsilon_{q\pm}^{\{k\}}(k_d,k_a;\Omega_{\rm lab})$ is the geometric factor; $S(J_i,\Lambda_i,J_e,\Lambda_e,J_f,\Lambda_f)$ is the product of reduced matrix elements of the dipole moments operator; and $h(k_d,k_a,k,J_i,J_e,J_f)$ contains the angular momentum coupling terms. The importance and meanings of these terms are discussed in KSZ1. We note that the values of J_e, Λ_e, J_f, and Λ_f are subject to the usual dipole selection rules which are contained in $S(J_i,\Lambda_i,J_e,\Lambda_e,J_f,\Lambda_f)$.

TABLE I. Nomenclature for the LIF transition strength formula.

J_i	= Rotational quantum number of the "initial"/ground state apart from nuclear spin
J_e	= Rotational quantum number of the "excited'/one photon state apart from nuclear spin
J_f	= Rotational quantum number of the "final"/lower state apart from nuclear spin
Λ_i	= Orbital angular momentum quantum number of the initial state
Λ_e	= Orbital angular momentum quantum number of the excited state
Λ_f	= Orbital angular momentum quantum number of the final state
k_a	= The rank for the square of the first (absorbed) photon
k_d	= The rank for the square of the second (detected) photon
k	= The rank for the ground state distribution
q	= The component for the ground state distribution
Ω	= Angles describing the geometry of the laser beam with respect to the coordinate system for the moments of the ground state distribution
θ_a,ϕ_a,χ_a	= Euler angles which rotate the lab into the probe/absorption frame
θ_d,ϕ_d,χ_d	= Euler angles which rotate the lab into the detector frame
$d^k_{q',q}(\theta)$	= The reduced rotation matrix element of angle θ
$\hat{\mathbf{B}}_a$	= The vector along which the probe light is linearly polarized before passing through the probe's quarter-wave plate.
$\hat{\mathbf{B}}_d$	= The vector parallel the major axis of the linear polarization of the detector
β_a	= Angle of the probe laser linear polarization vector with respect to the major axis of the probe's quarter-wave plate
β_d	= Angle of between the major axis of the quarter-wave plate and the linear polarizer of the detector
Δ_a	= Angle of the major axis of the probe's quarter-wave plate with respect to one of the three lab axis.
Δ_d	= Angle of the major axis of the quarter-wave plate of the detector with respect to one of the three lab axis.
F_i	= Total angular momentum quantum number of the ground state including nuclear spin.
F_e	= Total angular momentum quantum number of the excited state including nuclear spin.
I	= Nuclear spin quantum number
S	= Electronic spin quantum number
N_i	= Total angular momentum quantum number apart from spin of the ground state for Hund's case (b) molecules.
N_e	= Total angular momentum quantum number apart from spin of the excited state for Hund's case (b) molecules.

The brackets, { }, around the ranks of the tensors in Eqs. (1) and (2) indicate that we are employing the Hertel–Stoll[7] normalization for the spherical tensor operators. This forces all the $A_{q\pm}^{\{k\}}$ to be real. This normalization also reduces the number of detectable moments because often we can measure only the real or imaginary parts of the complex moments, $A_{\pm q}^{k}$. The transformation is straightforward:

$$T_{q+}^{\{k\}} = (-1)^q [2 - \delta_{q,0}]^{1/2} \,\mathrm{Re}[T_q^{(k)}]; \quad q \geqslant 0, \quad (3)$$

$$T_{q-}^{\{k\}} = (-1)^q [2]^{1/2} \,\mathrm{Im}[T_q^{(k)}]; \quad q > 0, \quad (4a)$$

$$T_{0-}^{\{0\}} = 0. \quad (4b)$$

The restrictions upon the use of Eqs. (3) and (4) are outlined in the Appendix of KSZ2.

The definitions of all the terms in Eqs. (1) and (2) are

explicitly given in Table I and are identical to those derived in KSZ1 and KSZ2 except the $J_{e'}$ has been replaced by J_e and $\Lambda_{e'}$ by Λ_e because the sum over excited state quantum numbers has been removed. The general formula for the geometric term, $\epsilon_q^{(k)}(k_d,k_a;\Omega_{\rm lab})$, for LIF is the same as that given in Table II of KSZ2, but the computed values are quite different because in LIF the two photons propagate along different directions, while in two-photon nonresonant absorption they are identical. The derivation of the equations for the geometric factor for the general case and for the special cases are given in the Appendix.

III. THE GEOMETRIC FACTOR AND THE SPECIAL GEOMETRIES

We present the equations for the geometric factor in order that we may identify the angles which specify the polarizations of the excitation light and of the fluorescence which is transmitted by the polarization analyzer. For all geometries:

$$\epsilon_q^{(k)}(k_d,k_a;\Omega_{\rm lab}) = \sum_m (-1)^{k_a-k_d-q}(2k+1)^{1/2} \times \begin{pmatrix} k_d & k_a & k \\ m & q-m & -q \end{pmatrix} \times E^{k_d}_m(\beta_d,\text{lab}) E^{k_a}_{q-m}(\beta_a,\text{lab}), \quad (5)$$

where

$$E^k_q(\beta,\text{lab}) = \sum_{q'} e^{iq'\chi} d^k_{q',q}(-\theta)\, e^{iq\phi} E^k_{q'}(\beta,\text{det/abs}), \quad (6a)$$

$E^k_q(\beta,\text{det/abs}) = [e^{*(1)} \otimes e^{(1)}]^k_q$, (χ,θ,ϕ) are the Euler angles which rotate the lab into the detector/absorption frames; $d^k_{q',q'}(-\theta)$ is a reduced rotation matrix element; β_a and β_d are the ellipticities of the absorbed photons and the detected photons which are transmitted by the polarization analyzer. Equations (5) and (6a) merely couple the electric field vectors of the absorbed and emitted photons. First, E^k_q is a spherical tensor element of the cross product of the electric field vector, $e^{(1)}$, with its complex conjugate, $e^{*(1)}$ (see KSZ2 for an explanation upon the calculation of this complex conjugate). Second, Eq. (5) couples together the E^k_q for the absorbed and detected photons; note that the summation in Eq. (5) over m is a summation over all the components of the E^k_q. To calculate the geometric factor in the Hertel–Stoll normalization, Eq. (5) is substituted into Eqs. (3) and (4).

For all cases, the Euler angles specify the position of the major axis of the ellipticity of the light relative to the fixed laboratory reference frame (see Fig. 1). Therefore, the Euler angles (ϕ_a,θ_a,χ_a) give the position of the major axis of the quarter-wave plate which prepares the absorbed photon, while (ϕ_d,θ_d,χ_d) describe the position of the quarter-wave plate in the detector. Note that the emitted light passes first through a quarter-wave plate, then a linear polarizer before reaching the detector.

In the general case (case A) the light propagates along the $-z_a$ ($-z_d$) axis and the major axis of the quarter-wave plate lies along x_a (x_d). We assume that the absorption light is linearly polarized along a vector $\hat{\mathbf{B}}_a$ before passing through the quarter-wave plate. β_a is defined as the angle between $\hat{\mathbf{B}}_a$ and x_a. We assume that the emitted light is passed through a linear polarizer after propagating through the quarter-wave plate and that the major axis of the linear

TABLE II. The laser induced fluorescence transition probability for noncoincident lab and detector frames where the detection geometry is general.

$$I = C(\text{det})n(J_i)\sum_{k,q,J_f}[P^{\{k\}}_{q+}(J_i,\Lambda_i,J_e,\Lambda_e,J_f,\Lambda_f;\Omega)A^{\{k\}}_{q+}(J_i) + P^{\{k\}}_{q-}(J_i,\Lambda_i,J_e,\Lambda_e,J_f,\Lambda_f;\Omega)A^{\{k\}}_{q-}(J_i)]$$

$$P^{\{k\}}_{q\pm}(J_i,\Lambda_i,J_e,\Lambda_e,J_f,\Lambda_f;\Omega) = b^k(J_i)g^k(J_i)g^k(J_e)\sum_{k_a,k_e}[(-1)^{(k)}\epsilon^{\{k\}}_{q\pm}(k_d,k_a;\Omega_{\rm lab}) \times S(J_i,\Lambda_i,J_e,\Lambda_e,J_f,\Lambda_f)h(k_d,k_a,k,J_i,J_e,J_f),$$

where $k = 0,1,2,3,4$; $q = 0,1,2,3,4$, but $q \le k$; $k_d = 0,1,2$; $k_a = 0,1,2$.

$$A^{\{k\}}_{q\pm}(J_i) = c(k)\langle(J_iM_i\Lambda_i|J^{\{k\}}_{q\pm}|J_iM_i\Lambda_i)\rangle/[(J_iM_i\Lambda_i|\mathbf{J}^2|J_iM_i\Lambda_i)]^{k/2}$$

$$\epsilon^{\{k\}}_{q+}(k_d,k_a;\Omega_{\rm lab}) = (-1)^q[2-\delta_{q,0}]^{1/2}\,\text{Re}[\epsilon^{(k)}_{+q}(k_d,k_a;\Omega_{\rm lab})]; \quad q>0$$

$$\epsilon^{\{k\}}_{q-}(k_d,k_a;\Omega_{\rm lab}) = (-1)^q(2)^{1/2}\,\text{Im}[\epsilon^{(k)}_{-q}(k_d,k_a;\Omega_{\rm lab})]; \quad q>0$$

$$\epsilon^{(k)}_q(k_d,k_a;\Omega_{\rm lab}) = \sum_m (-1)^{k_a-k_d-q}(2k+1)^{1/2} \times \begin{pmatrix} k_d & k_a & k \\ m & q-m & -q \end{pmatrix} E^{k_d}_m(\text{lab})E^{k_a}_{q-m}(\text{lab})$$

$$E^k_q(\text{lab}) = \sum_{q'} e^{iq'\chi}d^k_{q',q}(-\theta)e^{iq\phi}E^k_{q'}(\text{det})$$

$$E^k_q(\text{det}) = [e^{*(1)} \otimes e^{(1)}]^k_q$$

$n(J_i)$ = population of level J_i

$$b^k(J_i) = c(k)^{-1}\{[(J_iM_i\Lambda_i|\mathbf{J}^2|J_iM_i\Lambda_i)]^{k/2}\}/(J_i||J^{(k)}||J_i)$$

$$g^k(J_i) = \sum_T\sum_{F_i}(2F_i+1)^2\begin{Bmatrix} F_i & F_i & k \\ J_i & J_i & I \end{Bmatrix}^2$$

$$g^k(N_i) = \sum_{J_i}(2J_i+1)^2\begin{Bmatrix} J_i & J_i & k \\ N_i & N_i & S \end{Bmatrix}^2 g^k(J_i)$$

$$S(J_i,\Lambda_i,J_e,\Lambda_e,J_f,\Lambda_f) = |(J_e\Lambda_e||r^{(1)}||J_i\Lambda_i)|^2|(J_f\Lambda_f||r^{(1)}||J_e\Lambda_e)|^2$$

$$(J_2\Lambda_2||r^{(1)}||J_1\Lambda_1) = (4\pi/3)^{1/2}R^{(\Lambda_2-\Lambda_1)}_{21}(2J_2+1)^{1/2}(2J_1+1)^{1/2} \times (-1)^{(J_2-\Lambda_2)}\begin{pmatrix} J_1 & J_2 & 1 \\ \Lambda_1 & -\Lambda_2 & \Lambda_2-\Lambda_1 \end{pmatrix}$$

$$(J_2\Lambda_2||r^{(1)}||J_1\Lambda_1)^* = (-1)^{(J_2-J_1)}(J_1\Lambda_1||r^{(1)}||J_2\Lambda_2)$$

$$h(k_d,k_a,k,J_i,J_e,J_f) = (-1)^{(J_f+J_e-k_d+1)}[(2k_d+1)(2k_a+1)(2k+1)]^{1/2} \times \begin{Bmatrix} J_e & J_e & k_d \\ 1 & 1 & J_f \end{Bmatrix}\begin{Bmatrix} J_e & 1 & J_i \\ J_e & 1 & J_i \\ k_d & k_a & k \end{Bmatrix}$$

For $c(k)$ and $v(k)$ see Table IV of KSZ2
For $A^{\{k\}}_{q\pm}(J_i)$ see Table V of KSZ2
For $b^k(J_i)$ see Table VI of KSZ2
The depolarization factors $g^k(J_i)$ and $g^k(N_i)$ appearing in this table are valid for molecule with Hund's case $(b)_{\beta J}$ coupling, but the former is also valid for Hund's case (a) coupling. For Hund's case $(b)_{\beta S}$ see Ref. 9.
$|(J_2\Lambda_2||r^{(1)}||J_1\Lambda_1)|^2$ is proportional to the Hönl–London factors so for almost all transition, these reduced matrix elements need not be calculated since they are reported in the literature.

polarizer lies along a vector $\hat{\mathbf{B}}_d$. β_d is defined as the angle between $\hat{\mathbf{B}}_d$ and x_d. Note that both β_a and β_d are positive when the quarter-wave plates are rotated in a counterclockwise direction (see Fig. 1). For the general case, propagation along $-z_a$ or $-z_d$, the equations in Table III for E_q^k (case A,det/abs) are employed along with Eq. (6a) and the appropriate Euler angles.

For case I geometry, the light is propagating along the $-z$ axis of the lab frame and ellipticity is created using a quarter-wave plate whose major axis lies in the laboratory x–y plane. Let Δ_a be defined as the angle between the major axis of the quarter-wave plate and the x axis of the lab frame. Note when $\beta_a = 0°$, Δ_a describes the direction of linear polarization for the absorbed photons. The detected photons propagate along the y direction of the lab frame and pass through a quarter-wave plate whose major axis lies in the laboratory x–z plane. Let Δ_d be defined as the angles between the major axis of the quarter-wave plate and the z axis of the lab frame (see Fig. 1). Hence, for case I geometry, Eq. (6a) and the E_q^k (case A, det/abs) are employed along with Euler angles of $(0°,0°,-\Delta_a)$ and $(-90°,90°,180°-\Delta_d)$. Alternatively, one uses the simplified equations given in Table III (see the Appendix of KSZ2 for the derivations):

$$E^{k_a}_{q_a}(\text{lab}) = E_q^k(\text{case A,lab});$$

$$E^{k_d}_{q_d}(\text{lab}) = E_q^k(\text{case C,lab}) \quad (\text{case I}). \tag{6b}$$

For case II geometry, the light is propagating along the $-x$ axis of the lab frame and ellipticity is created using a quarter-wave plate whose major axis lies is the laboratory y–z plane. Let Δ be defined as the angle between the major axis of the quarter-wave plate and the z axis of the lab frame. The detected photons propagate along the y direction of the lab photon and pass through a quarter-wave plate whose major axis lies in the laboratory x–z plane. Let Δ_d be defined as the angles between the major axis of the wave plate and the z axis of the lab frame (see Fig. 1). As a result, for case II geometry, Eq. (6a) and the E_q^k (case A, det/abs) are employed along with Euler angles, $(0°,90°,180°-\Delta_a)$ and $(-90°,90°,180°-\Delta_d)$. Alternatively, one uses the simplified equations given in Table III:

TABLE III. E_q^k for light propagating or detected along the $-z$ (case A), $-x$ (case B), and y (case C) axes.

$$E_q^k(\text{case A, lab}) = (\cos q\Delta - i\sin q\Delta)E_q^k(\text{case A,det/abs})$$

$$E_q^k(\text{case B, lab}) = [\cos(q\pi/2) + i\sin(q\pi/2)]\sum_{q'} d^k_{q',q}(-\Delta) \times [\cos(q'\pi/2) - i\sin(q'\pi/2)]E_{q'}^k \ (\text{case B,det/abs})$$

$$E_q^k\ (\text{case C,lab}) = \sum_{q'} d^k_{q',q}(\Delta)E_q^k\ (\text{case C,det/abs})$$

The electric field vector cross products, E_q^k(det/abs), for light prepared with a quarter-wave plate

E_q^k	Case A	Case B	Case C
E_0^0	$-1/\sqrt{3}$	$-1/\sqrt{3}$	$-1/\sqrt{3}$
$E^1_{\pm 1}$	0	$(\pm 1/2)\sin 2\beta$	$(-i/2)\sin 2\beta$
E_0^1	$(-1/2)\sin 2\beta$	0	0
$E^2_{\pm 2}$	$(1/2)\cos 2\beta$	$(-1/2)\sin^2\beta$	$(1/2)\sin^2\beta$
$E^2_{\pm 1}$	0	0	0
E_0^2	$(-1/\sqrt{6})$	$(1/\sqrt{6})(3\cos^2\beta - 1)$	$(1/\sqrt{6})(3\cos^2\beta - 1)$

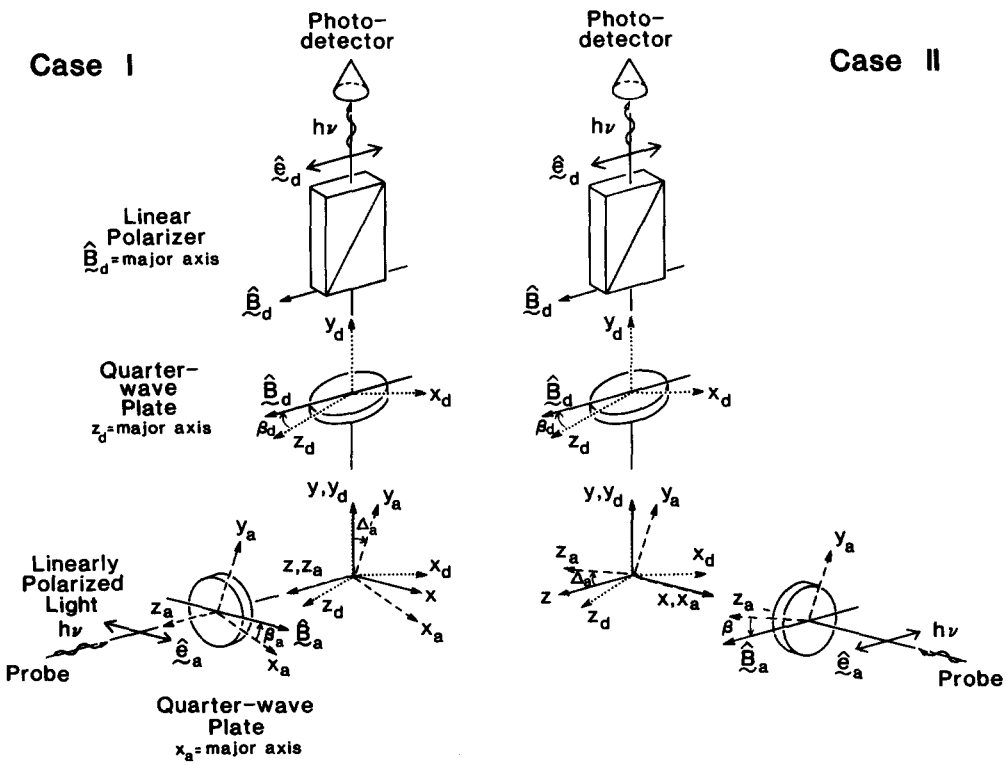

FIG. 1. The reference frames, angles, and electric field vector Cartesian components specific to: (a) case I geometry and (b) case II geometry.

$$E^{k_a}_{q_a}(\text{lab}) = E^k_q(\text{case B,lab});$$

$$E^{k_d}_{q_d}(\text{lab}) = E^k_q(\text{case C, lab}) \quad (\text{case II}). \tag{6c}$$

Table III also includes some very simple equations for the $E^k_q(\text{lab})$ which do not contain reduced matrix elements for two common experimental situations: (1) the light is linearly polarized; (2) the light is elliptically polarized but $\Delta = 0°$. To calculate the $E^k_q(\text{det})$ for unpolarized detection, we average over $\beta_d = 0°$ and 90°: $E^k_q(\text{unpolarized,det}) = [E^k_q(\beta = 0°,\text{det}) + E^k_q(\beta = 90°,\text{det})]/2$.

IV. THE UNREDUCED MOMENTS

In general, the rotational populations $n(J_i)$ and the detection sensitivity constant $C(\text{det})$ are unknown so we absorb these quantities into the polarization moments are rewrite Eq. (1) as follows:

$$I = \sum_{k,q,J_f} [P^{\{k\}}_{q+}(J_i,\Lambda_i,J_f,\Lambda_f;\Omega)a^{\{k\}}_{q+}(J_i) + P^{\{k\}}_{q-}(J_i,\Lambda_i,J_f,\Lambda_f;\Omega)a^{\{k\}}_{q-}(J_i)], \tag{7}$$

where

$$a^{\{k\}}_{q\pm}(J_i) = A^{\{k\}}_{q\pm}(J_i)n(J_i)C(\text{det}), \tag{8}$$

$$A^{\{k\}}_{q\pm}(J_i)/A^{\{0\}}_{0+}(J_i) = a^{\{k\}}_{q\pm}(J_i)/a^{\{0\}}_{0+}(J_i), \tag{9}$$

$$a^{\{0\}}_{0+}(J_i) = n(J_i)C(\text{det}), \tag{10}$$

$$A^{\{0\}}_{0+}(J_i) = 1. \tag{11}$$

Here, the $a^{\{k\}}_{q\pm}$ are the unreduced moments which are the ones that an experimentalist will determine from fitting the LIF intensities to the line strengths, $P^{\{k\}}_{q\pm}$. Equations (8)–(11) allow the determination of the reduced moments $A^{\{k\}}_{q\pm}/A^{\{0\}}_{0+}(J_i)$ and the rotational population $n(J_i)$ from the reduced moments.

V. DETERMINATION OF ALIGNMENT WITH UNPOLARIZED DETECTION

For linearly polarized excitation along an arbitrary direction there are 14 alignment moments which can be determined, $A^{\{k\}}_{q\pm}(J_i)$ with $k = 2,4$. Unfortunately, in order to measure independently all the moments we would need to vary the propagation direction of the excitation light. By restricting the electric field vector of the excitation light to a single plane of space, the $P^{\{k\}}_{q\pm}(J_i)$ lose their strict independence. This is apparent in Fig. 2 where $P^{\{k\}}_{q\pm}$ vs Δ_a is plotted for the LIF of the $B\,^2\Sigma$–$X\,^2\Sigma^+$ states of CN for case I geometry; the corresponding plots for case II geometry are shown in Fig. 3.

For case I geometry, note the similarity (same shape to within a constant) of the plots for $(k,q) = (2,2-)$, $(4,2-)$, and $(4,4-)$. In addition, for case I geometry, the plots for $(k,q) = (2,0+)$, $(4,4+)$, $(4,2+)$, and $(4,0+)$ look like a linear combination of the plots for (k,q)

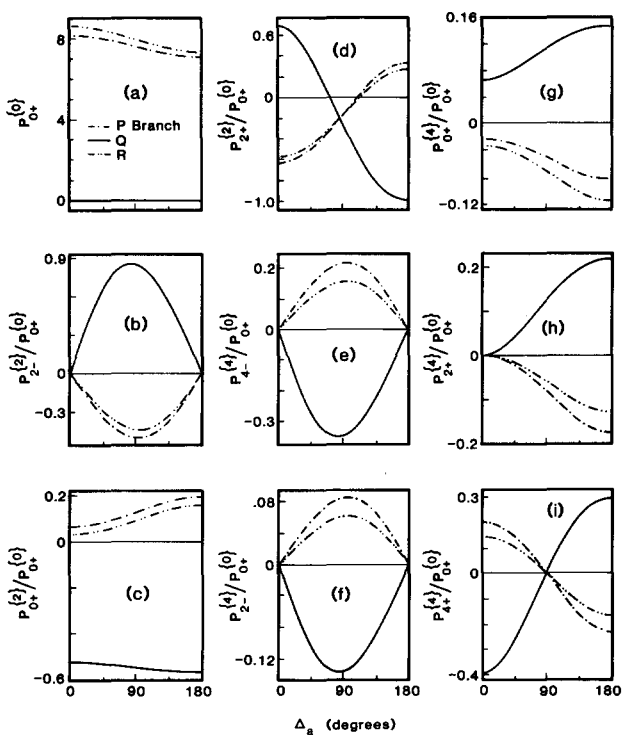

FIG. 2. The moments of the line strength factors $P^{\{k\}}_{0+}$ for case I geometry vs the angle of linear polarization Δ_a for the three principal absorption rotational branches of $J_i = 20$ at $\beta_a = 0°$ in the LIF of CN ($^2\Sigma$–$^2\Sigma$–$^2\Sigma$). We have assumed that the fluorescence is not dispersed and is collected independent of its polarization and that the CN has Hund's case $(b)_{\beta J}$ coupling (Ref. 13) in both the ground and excited states. The higher order moments have been normalized with respect to the zeroth moment.

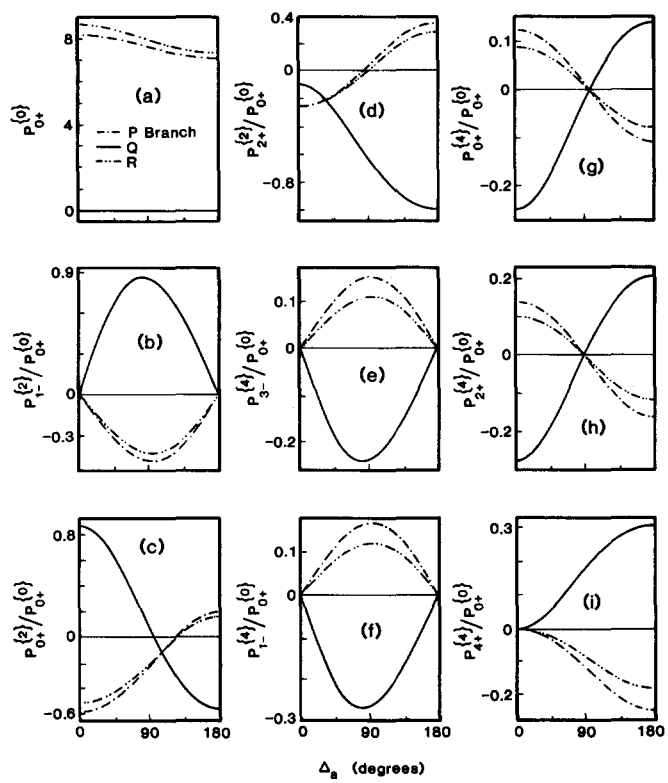

FIG. 3. The moments of the line strength factors $P^{\{k\}}_{0+}$ for case II geometry vs the angle of linear polarization Δ_a for the three principal absorption rotational branches of $J_i = 20$ at $\beta_a = 0°$ in the LIF of CN ($^2\Sigma$–$^2\Sigma$–$^2\Sigma$). We have assumed that the fluorescence is not dispersed and is collected independent of its polarization and that the CN has Hund's case $(b)_{\beta J}$ coupling (Ref. 13) in both the ground and excited states. The higher order moments have been normalized with respect to the zeroth moment.

$= (0,0+)$ and $(2,2+)$; in fact, for unpolarized detection, $P^{\{2\}}_{0+}(J_i,\Lambda_i,J_f,\Lambda_f;\Omega)$, $P^{\{4\}}_{4+}(J_i,\Lambda_i,J_f,\Lambda_f;\Omega)$, $P^{\{4\}}_{2+}(J_i,\Lambda_i,J_f,\Lambda_f;\Omega)$, and $P^{\{4\}}_{0+}(J_i,\Lambda_i,J_f,\Lambda_f;\Omega)$ are equal to a weighted sum of $P^{\{0\}}_{0+}(J_i,\Lambda_i,J_f,\Lambda_f;\Omega)$ and $P^{\{2\}}_{2+}(J_i,\Lambda_i,J_f,\Lambda_f;\Omega)$. Hence, for a fixed propagation direction, we can no longer independently determine the real moments, $a^{\{k\}}_{q\pm}(J_i)$, but only the apparent moments, $a^{\{k\}}_{q\pm}(J_i)$(app). These apparent moments are simple sums of real moments (see the Appendix of KSZ2):

$$P^{\{k\}}_{q\pm}(J_i,J_e,J_f;\Omega)(\text{dep}) = \sum_{k',q'} c(k,q,k',q',J_i,J_e,J_f)P^{\{k'\}}_{q'\pm}(J_i,J_e,J_f;\Omega)(\text{ind}); \tag{12a}$$

hence

$$I = \sum_{k,q,J_f}[P^{\{k\}}_{q+}(J_i,\Lambda_i,J_e,\Lambda_e,J_f,\Lambda_f;\Omega)a^{\{k\}}_{q+}(J_i,J_e)(\text{app}) + P^{\{k\}}_{q-}(J_i,\Lambda_i,J_e,\Lambda_e,J_f,\Lambda_f;\Omega)a^{\{k\}}_{q-}(J_i,J_e)(\text{app})], \tag{12b}$$

where

$$A^{\{k\}}_{q\pm}(J_i)(\text{app}) = \sum_{k',q'} c(k',q',k,q,J_i,J_e,J_f)A^{\{k'\}}_{q'\pm}(J_i,J_e). \tag{12c}$$

The expansion coefficients $c(k',q',k,q,J_i,J_e,J_f)$ in Eq. (12a) are specific to each geometry, to each rotational branch, and to linearly polarized light ($\beta_a = 0°$). Equation (12b) is derived by substituting Eq. (12a) into Eq. (7) and grouping the $a^{\{k\}}_{q\pm}$ as prescribed by Eq. (12c). The expansion coefficients are projections of the $P^{\{k\}}_{q\pm}(J_i)$(dep) onto the $P^{\{k\}}_{q\pm}(J_i)$(ind) where (ind) indicates the line strengths of the designated apparent moments and (dep) indicates a line strength of a moment which has not been designated as an apparent moment and is being expressed as the weighted sum of the $P^{\{k\}}_{q\pm}$(ind).

The coefficients can be derived numerically by using a linear least squares fit to Eq. (12a) or analytically by multiplying both sides of Eq. (12a) by $P^{\{k'\}}_{q'\pm}$ and integrating over the planes in which the electric field vectors rotate [see Eq. (A24) of KSZ2]. For LIF the analytical method is not useful [unlike the analytical method for $2+n$ REMPI given in Eq. (A24) of KSZ2] because the the parts of $e^{(k)}_q$ which depend on Δ cannot be separated from the parts which depend on k_a and k_d. Hence, Eq. (12a) has been numerically solved to derive the coefficients presented in Table IV.

It is important to note that although $A^{\{0\}}_{0+} = 1$, $A^{\{0\}}_{0+}(\text{app}) \neq 1$. We also note that all the experimentally determined reduced apparent moments, $A^{\{k\}}_{q\pm}(\text{app})$, have been normalized by $A^{\{0\}}_{0+}(\text{app})$ [see Eq. (9)]. Consequent-

TABLE IV. The apparent moments as a function of the reduced moments of the ground state distribution for $J = 20$ for a heteronuclear diatomic molecule (CN) with case (b) coupling and $I = 1$ undergoing $^2\Sigma$-$^2\Sigma$-$^2\Sigma$ LIF with unresolved emission. Note that the definitions of two of the apparent orientation moments, $A^{\{0\}}_{0+}(\text{app})$ and $A^{\{2\}}_{2+}(\text{app})$ (case I) or $A^{\{2\}}_{0+}(\text{app})$ (case II), are identical to the corresponding apparent alignment moments. The definitions for $A^{\{2\}}_{2-}(\text{app})$(case I) and $A^{\{2\}}_{1-}(\text{app})$(case II) apply only for alignment measurements. The definitions for $A^{\{1\}}_{0+}(\text{app})$(case I) and $A^{\{1\}}_{1+}(\text{app})$(case II) apply only for orientation measurements.

Case I geometry

$A^{\{0\}}_{0+}(\text{app}) = A^{\{0\}}_{0+} + 0.150A^{\{2\}}_{0+} - 0.081A^{\{4\}}_{4+} - 0.113A^{\{4\}}_{2+} - 0.087A^{\{4\}}_{0+}$	(P branch)
$A^{\{0\}}_{0+}(\text{app}) = A^{\{0\}}_{0+} - 0.539A^{\{2\}}_{0+} - 0.103A^{\{4\}}_{4+} + 0.092A^{\{4\}}_{2+} + 0.100A^{\{4\}}_{0+}$	(Q branch)
$A^{\{0\}}_{0+}(\text{app}) = A^{\{0\}}_{0+} + 0.117A^{\{2\}}_{0+} - 0.067A^{\{4\}}_{4+} - 0.085A^{\{4\}}_{2+} - 0.065A^{\{4\}}_{0+}$	(R branch)
$A^{\{2\}}_{2+}(\text{app}) = A^{\{2\}}_{2+} + 0.129A^{\{2\}}_{0+} - 0.438A^{\{4\}}_{4+} - 0.177A^{\{4\}}_{2+} - 0.085A^{\{4\}}_{0+}$	(P branch)
$A^{\{2\}}_{2+}(\text{app}) = A^{\{2\}}_{2+} + 0.027A^{\{2\}}_{0+} - 0.402A^{\{4\}}_{4+} - 0.130A^{\{4\}}_{2+} - 0.049A^{\{4\}}_{0+}$	(Q branch)
$A^{\{2\}}_{2+}(\text{app}) = A^{\{2\}}_{2+} + 0.145A^{\{2\}}_{0+} - 0.362A^{\{4\}}_{4+} - 0.148A^{\{4\}}_{2+} - 0.071A^{\{4\}}_{0+}$	(R branch)
$A^{\{2\}}_{2-}(\text{app}) = A^{\{2\}}_{2-} - 0.161A^{\{4\}}_{2-} - 0.427A^{\{4\}}_{4-}$	(P branch)
$A^{\{2\}}_{2-}(\text{app}) = A^{\{2\}}_{2-} - 0.146A^{\{4\}}_{2-} - 0.385A^{\{4\}}_{4-}$	(Q branch)
$A^{\{2\}}_{2-}(\text{app}) = A^{\{2\}}_{2-} - 0.132A^{\{4\}}_{2-} - 0.350A^{\{4\}}_{4-}$	(R branch)
$A^{\{1\}}_{0+}(\text{app}) = A^{\{1\}}_{0+} - 0.214A^{\{3\}}_{2+} - 0.166A^{\{3\}}_{0+}$	(P branch)
$A^{\{1\}}_{0+}(\text{app}) = A^{\{1\}}_{0+} - 0.464A^{\{3\}}_{2+} - 0.360A^{\{3\}}_{0+}$	(Q branch)
$A^{\{1\}}_{0+}(\text{app}) = A^{\{1\}}_{0+} - 0.198A^{\{3\}}_{2+} - 0.153A^{\{3\}}_{0+}$	(R branch)

Case II geometry

$A^{\{0\}}_{0+}(\text{app}) = A^{\{0\}}_{0+} + 0.187A^{\{2\}}_{2+} - 0.171A^{\{4\}}_{4+} - 0.092A^{\{4\}}_{2+} - 0.053A^{\{4\}}_{0+}$	(P branch)
$A^{\{0\}}_{0+}(\text{app}) = A^{\{0\}}_{0+} - 0.633A^{\{2\}}_{2+} - 0.176A^{\{4\}}_{4+} + 0.018A^{\{4\}}_{2+} - 0.014A^{\{4\}}_{0+}$	(Q branch)
$A^{\{0\}}_{0+}(\text{app}) = A^{\{0\}}_{0+} + 0.148A^{\{2\}}_{2+} - 0.127A^{\{4\}}_{4+} - 0.071A^{\{4\}}_{2+} - 0.042A^{\{4\}}_{0+}$	(R branch)
$A^{\{2\}}_{0+}(\text{app}) = A^{\{2\}}_{0+} + 0.763A^{\{2\}}_{2+} - 0.293A^{\{4\}}_{4+} - 0.413A^{\{4\}}_{2+} - 0.320A^{\{4\}}_{0+}$	(P branch)
$A^{\{2\}}_{0+}(\text{app}) = A^{\{2\}}_{0+} + 0.613A^{\{2\}}_{2+} - 0.202A^{\{4\}}_{4+} - 0.357A^{\{4\}}_{2+} - 0.285A^{\{4\}}_{0+}$	(Q branch)
$A^{\{2\}}_{0+}(\text{app}) = A^{\{2\}}_{0+} + 0.789A^{\{2\}}_{2+} - 0.247A^{\{4\}}_{4+} - 0.345A^{\{4\}}_{2+} - 0.267A^{\{4\}}_{0+}$	(R branch)
$A^{\{2\}}_{1-}(\text{app}) = A^{\{2\}}_{1-} - 0.342A^{\{4\}}_{1-} - 0.301A^{\{4\}}_{3-}$	(P branch)
$A^{\{2\}}_{1-}(\text{app}) = A^{\{2\}}_{1-} - 0.309A^{\{4\}}_{1-} - 0.272A^{\{4\}}_{3-}$	(Q branch)
$A^{\{2\}}_{1-}(\text{app}) = A^{\{2\}}_{1-} - 0.280A^{\{4\}}_{1-} - 0.247A^{\{4\}}_{3-}$	(R branch)
$A^{\{1\}}_{1+}(\text{app}) = A^{\{1\}}_{1+} - 0.262A^{\{3\}}_{3+} - 0.068A^{\{3\}}_{1+}$	(P branch)
$A^{\{1\}}_{1+}(\text{app}) = A^{\{1\}}_{1+} - 0.568A^{\{3\}}_{3+} - 0.147A^{\{3\}}_{1+}$	(Q branch)
$A^{\{1\}}_{1+}(\text{app}) = A^{\{1\}}_{1+} - 0.242A^{\{3\}}_{3+} - 0.063A^{\{3\}}_{1+}$	(R branch)

ly, when a theoretician calculates the apparent moments of an ensemble using the equations in Table IV, the apparent moments need to be normalized by the theoretically computed $A_{0+}^{\{0\}}$ (app) before being compared to the experimentally determined $A_{q\pm}^{\{k\}}$ (app)/$A_{0+}^{\{0\}}$ (app).

In order to measure the apparent moments, the LIF intensity is recorded at several polarizations of the excitation laser (Δ_a); the fluorescence is collected independent of its polarization; and the positions of both the detector and the laser propagation axes are fixed. The apparent moments can then be calculated using a linear least squares fit:

$$\mathbf{I}(\Delta_n,J_i,J_e) = \underset{\sim}{\mathbf{P}}_{q\pm}^{\{k\}}(\Delta_n,J_i,J_e)\mathbf{a}_{q\pm}^{\{k\}}(\text{app})(J_i,J_e), \quad (13a)$$

where

$$n = 0 \rightarrow n_{\max}, \quad (13b)$$

$$(k,q) = (0,0+),(2,2-),(2,2+) \quad \text{(case I)}, \quad (13c)$$

$$(k,q) = (0,0+),(2,1-),(2,0+) \quad \text{(case II)}. \quad (13d)$$

Here a vector is indicated by boldface, and the rectangular array is denoted by a bold face symbol with a tilde. The horizontal variables are the ranks and components of the moments of the lines strength, while the vertical variables are the polarization angles and rotational branches [see Eqs. (23a)–(23d) of KSZ2]. The subscript on Δ_n indicates the measurement number. When determining apparent moments, each rotational line is analyzed separately; therefore, each measurement is done at a unique Δ_a. In Eq. (13b) $n_{\max}$ equals the number of polarization angles employed. For the remainder of this paper we will use this matrix notation.

The choice of apparent moments is not unique; for example, for case I geometry, one could calculate an $a_{0+}^{\{2\}}$ (app) instead of an $a_{2+}^{\{2\}}$ (app). We have chosen the $a_{q\pm}^{\{k\}}$ (app) which have the most distinctive $P_{q\pm}^{\{k\}}$ in order to facilitate the measurement of the three $a_{q\pm}^{\{k\}}$ (app).

The ranks and components of the apparent moments are different for the two special geometries. When determining the apparent moments, we are trying to fit the data, which typically consist of many measurements, to only three parameters, the population and the two alignment moments. As a result, for this overdetermined system, we should obtain a small value of χ^2 (see Ref. 7). Here χ^2 is a quantification of the goodness of the fit of the experimental data to Eqs. (13a). By comparing these accurate apparent moments for different rotational branches, we can determine the sizes of the different real moments which constitute the apparent moments. Furthermore, we emphasize that a measurement of the intensity at just two polarization settings does not allow the determination of the apparent moments. Three measurements are required to calculate the three polarization moments, but many measurements are required in order to obtain meaningful values of χ^2.

Looking at the plot of $P_{0+}^{\{0\}}$ vs Δ_a in Figs. 2 and 3, one is struck by the fact that the monopole line strength is dependent on the probe's polarization. Hence, as is well known,[4] even when doing LIF on an isotropic, unpolarized sample, the intensity of emitted light will vary with Δ_a. This is because the excitation creates a polarized ensemble in the excited state and the emission from the anisotropic ensemble is viewed along one direction. If one collected all the fluorescence (one-photon absorption spectroscopy), performed multiphoton ionization (see Fig. 3 of KSZ1), or used a polarization analyzer before the detector, then $P_{0+}^{\{0\}}$ would be independent of Δ_a.

VI. DETERMINATION OF ORIENTATION WITH UNPOLARIZED DETECTION

For elliptically polarized excitation along an arbitrary direction, there are ten orientation moments that can be determined: the $A_{q\pm}^{\{k\}}(J_i)$ with $k = 1,3$. Once we restrict ourselves to a single rotational branch, a single propagation direction, a single Δ_a, and unpolarized detection along a fixed axis, we can measure only the apparent orientation moments because the $P_{q\pm}^{\{k\}}(J_i)$ have lost their strict independence. This can be seen in Fig. 4 where $P_{q\pm}^{\{k\}}$ vs β_a is plotted for the LIF of the $B\,^2\Sigma$–$X\,^2\Sigma^+$ states of CN for case I geometry. The corresponding plots for case II geometry are shown in Fig. 5.

For case I, note the similarity of the plots for $(k,q) = (1,0+)$, $(3,0+)$, and $(3,2+)$. In addition, the moments with even ranks look quite similar. The case I plots for $(k,q) = (2,0+)$, $(4,4+)$, $(4,2+)$, and $(4,0+)$ look like a linear combination of the plots for $(k,q) = (0,0+)$ and $(2,2+)$. Note that since $\Delta_a = 0°$, the case I line strengths for $(k,q) = (2,2-)$, $(4,2-)$, and $(4,4-)$ are zero. Consequently, under the aforementioned conditions, we can determine only apparent moments, $a_{q\pm}^{\{k\}}(J_i)$(app). These apparent moments include both alignment ($k = 0,2,4$) and orientation ($k = 1,3$) moments because both types contribute to the LIF signal when probing with

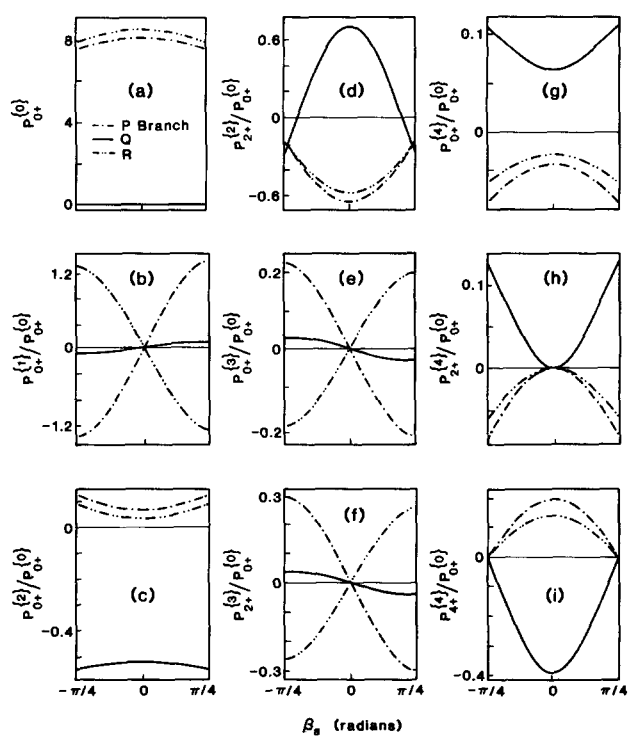

FIG. 4. The moments of the line strength factors $P_{0+}^{\{k\}}$ for case I geometry vs the ellipticity of the radiation β_a for the three principal absorption rotational branches of $J_i = 20$ at $\Delta_a = 0°$ in the LIF of CN ($^2\Sigma$–$^2\Sigma$). We have assumed that the fluorescence is not dispersed and is collected independent of its polarization and that the CN has Hund's case (b)$_{\beta J}$ coupling (Ref. 13) in both the ground and excited states. The higher order moments have been normalized with respect to the zeroth moment.

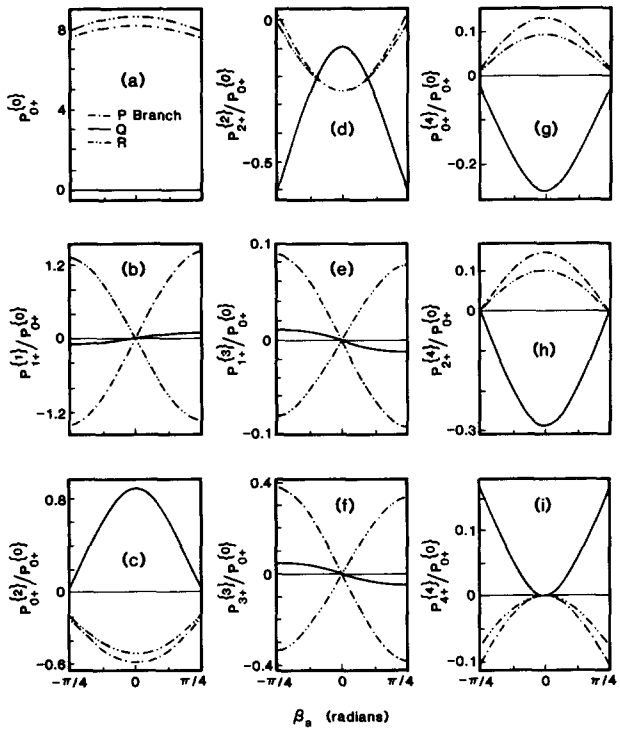

FIG. 5. The moments of the line strength factors $P_{0+}^{\{k\}}$ for case II geometry vs the ellipticity of the radiation β_a for the three principal absorption rotational branches of $J_i = 20$ at $\Delta_a = 0°$ in the LIF of CN ($^2\Sigma$–$^2\Sigma$–$^2\Sigma$). We have assumed that the fluorescence is not dispersed and is collected independent of its polarization and that the CN has Hund's case (b)$_{\beta J}$ coupling (Ref. 13) in both the ground and excited states. The higher order moments have been normalized with respect to the zeroth moment.

elliptically polarized light. We will refer to apparent moments for orientation experiments as "the apparent orientation moments," but this does not imply that only orientation moments ($k = 1,3$) are being measured.

The apparent orientation moments are once again simple sums of real moments; the expansion coefficients [see Eq. (12b)] are derived in the Appendix and given in Table IV. Note that the apparent orientation moments have different defintions from the apparent alignment moments (see Table IV). To fit the data from an experiment of LIF intensity vs β_a, Eq. (13a) can be employed to calculate the reduced apparent orientation moments. However, when using Eq. (13a) to determine orientation: $(k,q) = (0,0+)$, $(1,0+)$, and $(2,2+)$ for case I and $(k,q) = (0,0+)$, $(1,1+)$, $(2,0+)$ for case II. Note, for case I, $A_{0+}^{\{2\}}$ contributes to $A_{2+}^{\{2\}}$ (app) and, for case II, $A_{2+}^{\{2\}}$ contributes very strongly to $A_{0+}^{\{2\}}$ (app); hence, even when the ensemble being probed has only limited angular momentum anisotropy, it is very likely that none of the apparent orientation moments are zero. For example, in case I geometry, if there is cylindrical symmetry about the z axis, $A_{2+}^{\{2\}} = 0$, but $A_{0+}^{\{2\}} \neq 0$, hence $A_{2+}^{\{2\}}$ (app) $\neq 0$.

Alternatively, if $a_{0+}^{\{0\}}$ is known, the best way to analyze scans of intensity vs ellipticity is to examine at the difference between pairs of intensity measurements taken at $\pm\beta_a$ and to subtract the two intensities in order to calculate a "delta intensity", $\Delta I(\beta_a) = I(+\beta_a) - I(-\beta_a)]/2$, which is independent of the alignment since all the alignment moments have line strength which are identical at $\pm\beta_a$:

$$\Delta \mathbf{I}(\beta_n,J_i,J_e) = \underset{\sim}{\mathbf{P}}_{q\pm}^{\{k\}}(\beta_n,J_i,J_e)\mathbf{a}_{q\pm}^{\{k\}}(\text{app})(J_i,J_e), \tag{14a}$$

where

$$n = 0 \rightarrow n_{\max}, \tag{14b}$$

$$(k,q) = (1,0+) \quad \text{(case I)}, \tag{14c}$$

$$(k,q) = (1,1+) \quad \text{(case II)}. \tag{14d}$$

To obtain the orientation moments from Eq. (14a), Eq. (9) is subsequently employed. Once again, the multiple measurements will permit a meaningful error analysis of the experiment. This is not equivalent to just taking data at $\beta_a = \pm 45°$. When detecting orientation moments with unresolved fluorescence, measurements on the P and R branches serve as a check because they have orientation line strengths of nearly equal magnitude but of opposite sign. Measurements on the Q branch are rarely useful since the corresponding orientation line strengths are very small.

VII. DETECTION OF POLARIZATION FOR LIF WITH A $\Delta\Lambda = \pm 1$ TRANSITION

The detection of alignment and orientation using unpolarized fluorescence is quite similar for LIF of the $^2\Pi$–$^2\Sigma^+$ states as compared to LIF of the $^2\Sigma$–$^2\Sigma^+$ states when we assume all states have Hund's case (b) coupling. We use the same set of apparent moments, but the $c(k',q',k,q,J_i,J_e)$ are slightly different [see Eq. (13)]. In Table V, we present the apparent moments for $^2\Pi$–$^2\Sigma$ transitions for the case in which both the ground and excited states obey Hund's case (b) coupling.

The formulas to calculate the line strength are the same except for $S(J_i,\Lambda_i,J_e,\Lambda_e,J_f,\Lambda_e)$, the product of the Hönl–London factors connecting the ground state with excited state and the excited state with the final state. The alignment and orienation line strengths for $\Delta\Lambda = \pm 1$ transitions have nearly identical shapes but different magnitudes (factor of 1/2 to 2.0) than those for $\Delta\Lambda = 0$ transition. Not only are all the equations presented in this paper valid for $\Delta\Lambda = \pm 1$ transition (except the specific expansion coefficient for the apparent moments), but Figs. 2–7 give a reasonable good insight into how the line strength for $\Delta\Lambda = \pm 1$ transitions vary with probe laser polarization.

Most multiplet Π states only exhibit Hund's case (b) coupling for very high rotational states. Hence, to calculate accurate line strengths, the wave functions for a state with intermediate coupling must be employed. In general, to calculate the line strengths, a detailed knowledge of the fine structure energy level splittings of all rotational states is required.[10] However for $^2\Pi$ states, we need only to know a single constant,[11] $Y = A/B$ (called λ in Refs. 11 and 12) in order to calculate the wave functions of all the rotational states. For a $^2\Pi$–$^2\Sigma$ or a $^2\Sigma$–$^2\Pi$ transition, once the Y value is known, it is straightforward to calculate $S(J_i,\Lambda_i,J_e,\Lambda_e,J_f,\Lambda_e)$ since the Hönl–London factors can be readily evaluated.[11]

TABLE V. The apparent moments as a function of the reduced moments of the ground state distribution for $J = 20$ for a heteronuclear diatomic molecule (NO) with case (b) coupling and $I = 1$ undergoing $^2\Pi$–$^2\Sigma$–$^2\Pi$ LIF with unresolved emission. Note that the definitions of two of the apparent orientation moments, $A_{0+}^{\{0\}}$ (app) and $A_{2+}^{\{2\}}$ (app) (case I) or $A_{0+}^{\{2\}}$ (app) (case II), are identical to the corresponding apparent alignment moments. The definitions for $A_{2-}^{\{2\}}$ (app) (case I) and $A_{1-}^{\{2\}}$ (app) (case II) apply only for alignment measurements. The definitions for $A_{0+}^{\{1\}}$ (app) (case I) and $A_{1+}^{\{1\}}$ (app) (case II) apply only for orientation measurements.

Case I geometry

$A_{0+}^{\{0\}}(\text{app}) = A_{0+}^{\{0\}} + 0.334 A_{0+}^{\{2\}} - 0.021 A_{4+}^{\{4\}} + 0.031 A_{2+}^{\{4\}} + 0.031 A_{0+}^{\{4\}}$	(R branch)
$A_{0+}^{\{0\}}(\text{app}) = A_{0+}^{\{0\}} - 0.453 A_{0+}^{\{2\}} - 0.030 A_{4+}^{\{4\}} - 0.079 A_{2+}^{\{4\}} - 0.066 A_{0+}^{\{4\}}$	(Q branch)
$A_{0+}^{\{0\}}(\text{app}) = A_{0+}^{\{0\}} + 0.301 A_{0+}^{\{2\}} - 0.017 A_{4+}^{\{4\}} + 0.021 A_{2+}^{\{4\}} + 0.022 A_{0+}^{\{4\}}$	(R branch)
$A_{2+}^{\{2\}}(\text{app}) = A_{2+}^{\{2\}} - 0.085 A_{0+}^{\{2\}} + 0.235 A_{4+}^{\{4\}} + 0.086 A_{2+}^{\{4\}} + 0.037 A_{0+}^{\{4\}}$	(P branch)
$A_{2+}^{\{2\}}(\text{app}) = A_{2+}^{\{2\}} - 0.023 A_{0+}^{\{2\}} + 0.215 A_{4+}^{\{4\}} + 0.087 A_{2+}^{\{4\}} + 0.042 A_{0+}^{\{4\}}$	(Q branch)
$A_{2+}^{\{2\}}(\text{app}) = A_{2+}^{\{2\}} - 0.100 A_{0+}^{\{2\}} + 0.196 A_{4+}^{\{4\}} + 0.071 A_{2+}^{\{4\}} + 0.031 A_{0+}^{\{4\}}$	(R branch)
$A_{2-}^{\{2\}}(\text{app}) = A_{2-}^{\{2\}} + 0.088 A_{2-}^{\{4\}} + 0.233 A_{4-}^{\{4\}}$	(P branch)
$A_{2-}^{\{2\}}(\text{app}) = A_{2-}^{\{2\}} + 0.080 A_{2-}^{\{4\}} + 0.212 A_{4-}^{\{4\}}$	(Q branch)
$A_{2-}^{\{2\}}(\text{app}) = A_{2-}^{\{2\}} + 0.073 A_{2-}^{\{4\}} + 0.194 A_{4-}^{\{4\}}$	(R branch)
$A_{0+}^{\{1\}}(\text{app}) = A_{0+}^{\{1\}} + 0.092 A_{2+}^{\{3\}} + 0.071 A_{0+}^{\{3\}}$	(P branch)
$A_{0+}^{\{1\}}(\text{app}) = A_{0+}^{\{1\}} + 0.306 A_{2+}^{\{3\}} + 0.237 A_{0+}^{\{3\}}$	(Q branch)
$A_{0+}^{\{1\}}(\text{app}) = A_{0+}^{\{1\}} + 0.083 A_{2+}^{\{3\}} + 0.065 A_{0+}^{\{3\}}$	(R branch)

Case II geometry

$A_{0+}^{\{0\}}(\text{app}) = A_{0+}^{\{0\}} + 0.368 A_{2+}^{\{2\}} + 0.061 A_{4+}^{\{4\}} + 0.017 A_{2+}^{\{4\}} + 0.005 A_{0+}^{\{4\}}$	(P branch)
$A_{0+}^{\{0\}}(\text{app}) = A_{0+}^{\{0\}} - 0.516 A_{2+}^{\{2\}} - 0.134 A_{4+}^{\{4\}} - 0.064 A_{2+}^{\{4\}} - 0.035 A_{0+}^{\{4\}}$	(Q branch)
$A_{0+}^{\{0\}}(\text{app}) = A_{0+}^{\{0\}} + 0.328 A_{2+}^{\{2\}} + 0.043 A_{4+}^{\{4\}} + 0.011 A_{2+}^{\{4\}} + 0.003 A_{0+}^{\{4\}}$	(R branch)
$A_{0+}^{\{2\}}(\text{app}) = A_{0+}^{\{2\}} + 0.470 A_{2+}^{\{2\}} + 0.125 A_{4+}^{\{4\}} + 0.195 A_{2+}^{\{4\}} + 0.154 A_{0+}^{\{4\}}$	(P branch)
$A_{0+}^{\{2\}}(\text{app}) = A_{0+}^{\{2\}} + 0.548 A_{2+}^{\{2\}} + 0.132 A_{4+}^{\{4\}} + 0.185 A_{2+}^{\{4\}} + 0.143 A_{0+}^{\{4\}}$	(Q branch)
$A_{0+}^{\{2\}}(\text{app}) = A_{0+}^{\{2\}} + 0.451 A_{2+}^{\{2\}} + 0.103 A_{4+}^{\{4\}} + 0.162 A_{2+}^{\{4\}} + 0.127 A_{0+}^{\{4\}}$	(R branch)
$A_{1-}^{\{2\}}(\text{app}) = A_{1-}^{\{2\}} + 0.187 A_{1-}^{\{4\}} + 0.165 A_{3-}^{\{4\}}$	(P branch)
$A_{1-}^{\{2\}}(\text{app}) = A_{1-}^{\{2\}} + 0.170 A_{1-}^{\{4\}} + 0.150 A_{3-}^{\{4\}}$	(Q branch)
$A_{1-}^{\{2\}}(\text{app}) = A_{1-}^{\{2\}} + 0.156 A_{1-}^{\{4\}} + 0.137 A_{3-}^{\{4\}}$	(R branch)
$A_{1+}^{\{1\}}(\text{app}) = A_{1+}^{\{1\}} + 0.113 A_{3+}^{\{3\}} + 0.029 A_{1+}^{\{3\}}$	(P branch)
$A_{1+}^{\{1\}}(\text{app}) = A_{1+}^{\{1\}} + 0.375 A_{3+}^{\{3\}} + 0.097 A_{1+}^{\{3\}}$	(Q branch)
$A_{1+}^{\{1\}}(\text{app}) = A_{1+}^{\{1\}} + 0.102 A_{3+}^{\{3\}} + 0.026 A_{1+}^{\{3\}}$	(R branch)

VIII. CORRELATIONS WITH VELOCITY

When the probe laser direction is fixed, the line strengths are no longer independent, and hence the determination of the bipolar harmonics between the velocity and polarization (line shape analysis) as described by Dixon[5] and Houston[8] is no longer possible. If the laser propagation direction is fixed and the fluorescence is collected without polarization filtering, then only apparent alignment moments, apparent velocity moments, and apparent bipolar moments can be detected. The determination of these apparent moments is postponed for future publication.

IX. DETECTION OF ALIGNMENT WITH POLARIZED DETECTION

In order to determine the real alignment moments instead of the apparent alignment moments, we must vary the propagation direction of the probe beam,[3] vary the position of the detector over all of space, or polarization analyze the polarization of the emitted photons. Experimental consideration almost always makes the last choice preferable. Since we are interested only in varying Δ_d while keeping β_d constant, we simultaneously rotate the detector quarter-wave plate and the linear polarizer while keeping their major axes parallel. Figure 6 depicts the line strengths for a "double delta scan", $P_{q\pm}^{\{k\}}$ vs Δ_a and Δ_d at $\beta_a = 0°$ and $\beta_d = 0°$. This is shown for the LIF of the $B\,^2\Sigma$–$X\,^2\Sigma^+$ states of CN for case I geometry. Experimentally, a double delta scan is acquired by measuring the LIF intensity vs Δ_a at various Δ_d. Note that we need only to vary Δ_d between 0° and 45° in order to span the space. We can directly use a linear least squares fit to Eq. (7) to determine the real moments:

$$\mathbf{I}(\Delta_n, J_i, J_e) = \underline{\mathbf{P}}_{q\pm}^{\{k\}}(\Delta_n, J_i, J_e)\,\mathbf{a}_{q\pm}^{\{k\}}(J_i), \tag{15a}$$

where

$$n = 0 \rightarrow n_{\max}, \tag{15b}$$

$$(k,q) = (0,0+),(2,2-),(2,0+),(2,2+) \quad (4,4-),(4,2-(,(4,0+),(4,2+),(4,4+) \quad \text{(case I)}, \tag{15c}$$

$$(k,q) = (0,0+),(2,1-),(2,0+),(2,2+) \quad (4,3-)(4,1-),(4,0+),(4,2+),(4,4+) \quad \text{(case II)}. \tag{15d}$$

In general, measurements at $n_{\max}$ polarization angles need to be taken, but if both a parallel and a perpendicular rotational branch can be probed, (for example, a P and a Q branch), then measurements at only $n_{\max}/2$ polarizations need be recorded. By varying the polarization of the detector, we can measure nine alignment moments as opposed to

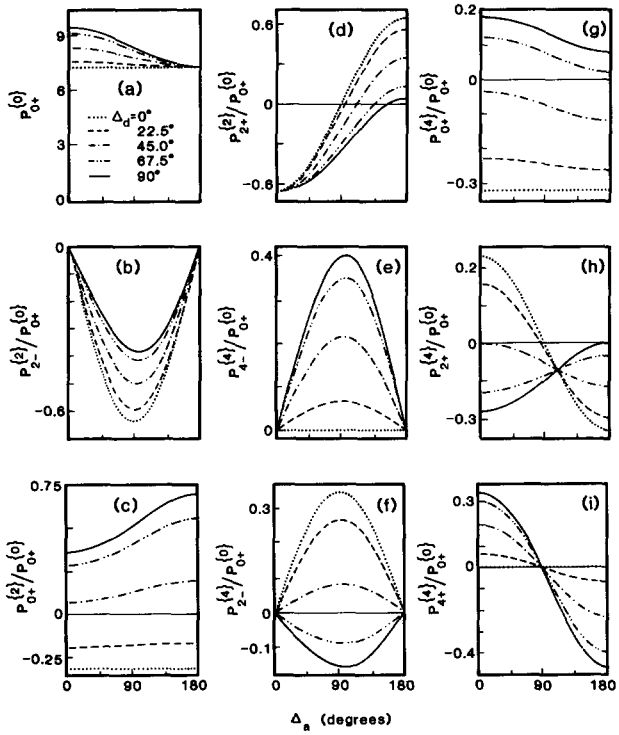

FIG. 6. "A double delta scan": The moments of the line strength factors $P_{0+}^{\{k\}}$ for case I geometry vs the angles of linear polarization of the probe light Δ_a and the emitted light Δ_d for the three principal absorption rotational branches of $J_i = 20$ at $\beta_a = 0°$ and $\beta_d = 0°$ in the LIF of CN ($^2\Sigma$-$^2\Sigma$-$^2\Sigma$). We have assumed that the fluorescence is not dispersed and that the CN has Hund's case (b)$_{\beta J}$ coupling (Ref. 13) in both the ground and excited states. The higher order moments have been normalized with respect to the zeroth moment.

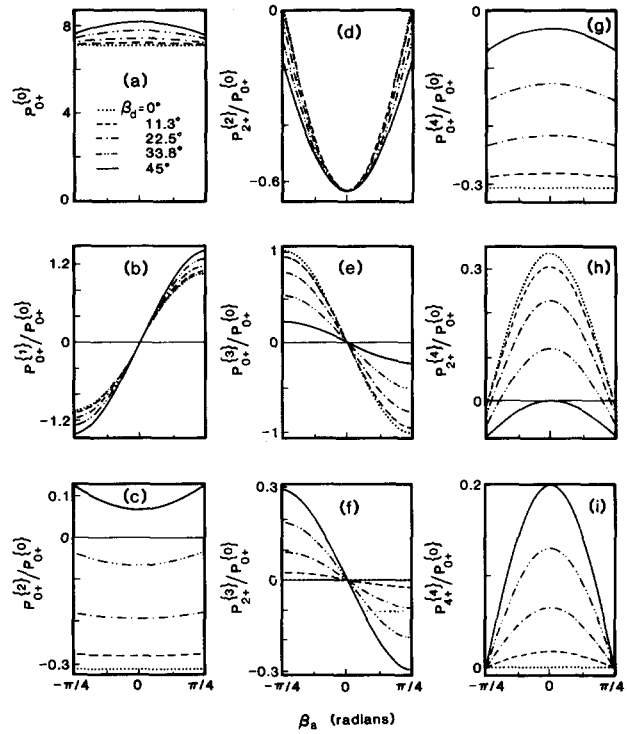

FIG. 7. "A double beta scan": The moments of the line strength factors $P_{0+}^{\{k\}}$ for Case I geometry vs the ellipticities of the radiation of the probe light β_a and the emitted light β_d for the three principal absorption rotational branches of $J_i = 20$ at $\Delta_a = 0°$ and $\Delta_d = 0°$ in the LIF of CN ($^2\Sigma$-$^2\Sigma$-$^2\Sigma$). We have assumed that the fluorescence is not dispersed and that the CN has Hund's case (b)$_{\beta J}$ coupling (Ref. 13) in both the ground and excited states. The higher order moments have been normalized with respect to the zeroth moment.

the three apparent moments that can be measured using unpolarized detection [see Eq. (13)]. The additional polarization moments can then be obtained by varying both the excitation and detection probe. This allows a more precise characterization of the anisotropy in the angular momentum distribution.

X. DETECTION OF ORIENTATION WITH POLARIZED DETECTION

For orientation, the analogue of the double delta scan is the "double beta scan". In order to independently measure multiple orientations with a fixed detector and probe directions, one can record the LIF intensity vs β_a at several β_d at fixed Δ_a and fixed Δ_d. This is accomplished by rotating the detector quarter-wave plate while keeping the linear polarizer of the detector fixed with its major axis along z. Figure 7 depicts the line strengths for a double beta scan, $P_{q\pm}^{\{k\}}$ vs β_a and β_d at $\Delta_a = 0°$ and $\Delta_d = 0°$ for the LIF of the $B\,^2\Sigma$-$X\,^2\Sigma^+$ states of CN for case I geometry. To determine the orientations, we carry out a linear least squares fit of "delta intensity" vs β_a and β_d where

$$\Delta I(\beta_a,\beta_d) = [I(+\beta_a) - I(-\beta_a)]/2,$$

$$\Delta \mathbf{I}(\Delta_n,J_i,J_e) = \underline{\mathbf{P}}_{q\pm}^{\{k\}}(\Delta_n,J_i,J_e)\mathbf{a}_{q\pm}^{\{k\}}(J_i), \quad (16a)$$

where

$$n = 0 \rightarrow n_{\max}, \quad (16b)$$

$$(k,q) = (1,0+),(3,0+),(3,2+) \quad \text{(case I)}, \quad (16c)$$

$$(k,q) = (1,1+),(3,1+),(3,3+) \quad \text{(case II)}. \quad (16d)$$

Additional orientation moments can be detected if $\Delta_a \neq 0°$ and $\Delta_d \neq 0°$: for case I the additional moments are $A_{1-}^{\{1\}}$ and $A_{1-}^{\{3\}}$ for the case II geometry the additional moments are $A_{0+}^{\{1\}}$, $A_{0+}^{\{3\}}$, and $A_{2+}^{\{3\}}$. When doing a double beta scan, $n_{\max}$ different ellipticities need to be employed since data from more than one branch are, in general, not useful (see discussion in Sec. VI). In comparing Eqs. (14) and (16), we note that varying the excitation and detection polarization ellipticity allows the determination of three orientation moments with $k = 1,3$ instead of one apparent orientation moment.

XI. DETECTION OF ALIGNMENT WITH MAGIC ANGLES

Sometimes it is impossible to scan the polarization of either the probed laser or the detection analyzer because the ensemble being probed is not stable for a reasonable period of time. Then one is forced to take measurements at just two polarizations with a device which rapidly switches (flips) the linear polarization or rapidly switches elliptical polarization from left circularly polarized light to right circularly polarized light (for example, using a photoelastic modulator). Unfortunately, this sort of measurement never permits determination of χ^2 thus preventing a meaningful error analysis because only two distinct measurements are being employed to determine two parameters, the population and one apparent polarization moment. Repeating these two measurements many times reduces the variance in the data, σ^2,

but does not give an indication as to how well the system is being modeled by the two parameters. A measure of the goodness of the fit of the model to the data, χ^2, can be obtained only from multiple independent measurements of LIF at several polarizations of the excitation light.

There are three ways to do magic angle measurements: (1) flip the polarization of the probe; (2) flip the polarization of the detection analyzer; and (3) flip alternately the polarization of the probe and the polarization of the detection analyzer. We will look only at the first case since this is the one which is most commonly implemented.

For unpolarized detection and a fixed probe and detection direction, we are sensitive only to two polarization moments. We can make measurements $I(\Delta_1)$ and $I(\Delta_2)$ at two incident linear polarizations, Δ_1 and Δ_2, for which one of the two polarization moments is zero (or nearly zero) at both angles. Comparing the two intensities with the known line strengths, we can calculate the polarization moments:

$$a_{0+}^{\{0\}}(\text{app}) = \frac{\{I(\Delta_1) - I(\Delta_2)\cdot[P_{q\pm}^{\{k\}}(\Delta_1)/P_{q\pm}^{\{k\}}(\Delta_2)]\}}{\{P_{0+}'^{\{0\}}(\Delta_1) - P_{0+}'^{\{0\}}(\Delta_2)\cdot[P_{q\pm}^{\{k\}}(\Delta_1)/P_{q\pm}^{\{k\}}(\Delta_2)]\}}, \tag{17a}$$

$$A_{q\pm}^{\{k\}}(\text{app}) = \frac{[I(\Delta_1) - I(\Delta_2)] - a_{0+}^{\{0\}}(\text{app})\cdot[P_{0+}'^{\{0\}}(\Delta_1) - P_{0+}'^{\{0\}}(\Delta_2)]}{a_{0+}^{\{0\}}(\text{app})\cdot[P_{q\pm}^{\{k\}}(\Delta_1) - P_{q\pm}^{\{k\}}(\Delta_2)]}, \tag{17b}$$

where

$$P_{q\pm}^{\{k\}} = P_{2+}^{\{2\}};\quad P_{0+}'^{\{0\}} = P_{0+}^{\{0\}};\quad \Delta_1 = 0°;\quad \Delta_2 = 90° \quad \text{(case I)}, \tag{17c}$$

$$P_{q\pm}^{\{k\}} = P_{0+}^{\{2\}};\quad P_{0+}'^{\{0\}} = P_{0+}^{\{0\}};\quad \Delta_1 = 0°;\quad \Delta_2 = 90° \quad \text{(case II)}, \tag{17d}$$

$$P_{q\pm}^{\{k\}} = P_{2-}^{\{2\}};\quad P_{0+}'^{\{0\}} = P_{0+}^{\{0\}} - A_{2+}^{\{2\}}\cdot P_{2+}^{\{2\}};\quad \Delta_1 = \sim 45°;\quad \Delta_2 = \sim -45° \quad \text{(case I)}, \tag{17e}$$

$$P_{q\pm}^{\{k\}} = P_{1-}^{\{2\}};\quad P_{0+}'^{\{0\}} = P_{0+}^{\{0\}} - A_{0+}^{\{2\}}\cdot P_{0+}^{\{2\}};\quad \Delta_1 = \sim 45°;\quad \Delta_2 = \sim -45° \quad \text{(case II)}. \tag{17f}$$

Here $P_{0+}'^{\{0\}}$ is used to account for any contributions to the intensity from $a_{0+}^{\{0\}}$ (app) and from other known polarization moments. In Eqs. (17c) and (17d), data are being recorded at magic angles so there are no contributions to the intensity from polarization moments other than the one being measured and $a_{0+}^{\{0\}}$ (app); in Eqs. (17e) and (17f), all polarization moments contribute to the intensity.

The exact angles to use in Eqs. (17e) and (17f) depend on J_i and J_e. With the help of the equations given in Table I, one calculates the line strength of $P_{2+}^{\{2\}}$ or $P_{0+}^{\{2\}}$ vs Δ_a to find the polarization at which $p_{2-}^{\{2\}} = 0$ or $P_{1-}^{\{2\}} = 0$. These are the Δ_a which we would like to use to determine $A_{2-}^{\{2\}}$ or $A_{1-}^{\{2\}}$. Some fast polarization switches (such as a photoelastic modulator operating alternatively as a zero-wave plate and a half-wave plate) can rotate linearly polarized light by an arbitrary angle. For this case, $\Delta_1 = \Delta$(magic angle 1) and $\Delta_2 = \Delta$ (magic angle 2), hence $P_{2+}^{\{2\}}(\Delta = \sim \pm 45°) = 0$, thus $P_{0+}'^{\{0\}}(\Delta = \sim \pm 45°) = P_{0+}^{\{0\}}(\Delta = \sim \pm 45°)$.

However, some fast polarization switchers can rotate the linear polarization only by 90°; consequently, we can employ the magic angles in Eqs. (17e) or (17f) only if the magic angles occur at $\Delta_a = \pm 45°$. Thus, we must settle for doing experiments slightly away from the magic angles when determining $A_{2-}^{\{2\}}$ or $A_{1-}^{\{2\}}$. $\Delta_a = \pm 45°$ are usually close to the magic angles and are, obviously, 90° apart.

Note that Eq. (17b) is not equivalent to the more familiar formula for determining the polarization: $P = [I(\|) - I(\perp)]/[I(\|) + I(\perp)]$. Here P is assumed to be proportional to $A_{2+}^{\{2\}}$ in case I geometry and $A_{0+}^{\{2\}}$ in case II geometry. This assumption is true only if all the fluorescence is collected (one photon absorption spectroscopy) or if a polarizer is used on the detector to insure that $P_{0+}^{\{0\}}$ is independent of the polarization of the probe (see Fig. 6). Even when these conditions are fulfilled, the constants which relate the degree of polarization P to the real polarization moments, $A_{2+}^{\{2\}}$ or $A_{0+}^{\{2\}}$, are functions of J_i and J_e:

$$A_{q\pm}^{\{k\}}(\text{app}) = \frac{P\cdot[P_{0+}^{\{0\}}(\Delta_1) + P_{0+}^{\{0\}}(\Delta_2)] - [P_{0+}^{\{0\}}(\Delta_1) - P_{0+}^{\{0\}}(\Delta_2)]}{[P_{q\pm}^{\{k\}}(\Delta_1) - P_{q\pm}^{\{k\}}(\Delta_2)] - P\cdot[P_{q\pm}^{\{k\}}(\Delta_1) + P_{q\pm}^{\{k\}}(\Delta_2)]}, \tag{18a}$$

where

$$(k,q) = (2,2+);\quad \Delta_1 = 0°;\quad \Delta_2 = 90° \quad \text{(case I)}, \tag{18b}$$

$$(k,q) = (2,0+);\quad \Delta_1 = 0°;\quad \Delta_2 = 90° \quad \text{(case II)}. \tag{18c}$$

Note that depending upon how $I(\|)$ and $I(\perp)$ are defined, $\Delta_1 = 0°, \pm 90°$ and $\Delta_2 = 0°, \pm 90°$. However, Eq. (18a) is valid only if the polarization ratio was measured at the magic angles, $\Delta = 0°, \pm 90°$. It is emphasized that reporting the degree of polarization is an inferior method of presenting data because it does not reduce the data to the expectation values of angular momentum operators.

Equations (17a)–(17f) determine all the apparent moments and consequently enable the experimentalist to record a single spectrum at one polarization and correct the measured intensities for the line strengths as a function of J_i and J_e as well as for any polarization effects. At a given Δ_a:

$$a_{0+}^{\{0\}}(J_i,J_e,\Delta_a)=\Big[I(J_i,J_e,\Delta_a)-\sum_{k,q}a_{q\pm}^{\{k\}}P_{q\pm}^{\{k\}}(J_i,J_e,\Delta_a)\Big]\Big/P_{0+}^{\{0\}}(J_i,J_e,\Delta_a), \tag{19a}$$

where

$$(k,q)=(2,2+),(2,2-) \quad \text{case I}, \tag{19b}$$

$$(k,q)=(2,0+),(2,1-) \quad \text{case II}. \tag{19c}$$

The experimentalist should choose Δ_a to minimize the contribution of the alignment to Eq. (19a). For example, in case I geometry, if the $a_{2-}^{\{2\}}$ is much smaller than $a_{2+}^{\{2\}}$ or in case II geometry, if the $a_{1-}^{\{2\}}$ is much smaller than $a_{0+}^{\{2\}}$, then Δ_a should be set at $\sim 45°$. The condition for case II geometry is always true when the system has cylindrical symmetry about the z axis.

The major problem with magic angle formulas is the lack of a meaningful error analysis. This can be overcome by checking the alignment moments with measurements at other pairs of linear polarizations (which can be 90° apart) and calculating one of the two apparent alignment moments assuming the other is known. To analyze this type of experiment, Eqs. (17a) and (17b) are used in conjunction with the following definition:

$$P'^{\{0\}}_{0+}(\Delta)=P_{0+}^{\{0\}}(\Delta)-A_{q'\pm}^{\{k'\}}(\text{app})P_{q'\pm}^{\{k'\}}(\Delta). \tag{20}$$

In Eqs. (17a), (17b), and (20), $A_{q\pm}^{\{k\}}(\text{app})$ is the apparent alignment moment which is being checked, while $A_{q'\pm}^{\{k'\}}(\text{app})$ is the apparent alignment moment which is assumed to be known.

XII. DETECTION OF ORIENTATION WITH MAGIC ANGLES

The determination of the orientation using magic angles is quite straightforward because "delta intensity" $\Delta I(\beta_a)=[I(+\beta_a)-I(-\beta_a)]/2$ depends only on the orientation moments since the alignment moments have equal line strengths at $+\beta_a$ and $-\beta_a$:

$$A_{q\pm}^{\{k\}}(\text{app})=\left(\frac{I(\beta_a)-I(-\beta_a)}{I(\beta_a)+I(-\beta_a)}\right)\times\left(\frac{P_{0+}^{\{0\}}(\beta_a)+A_{q'\pm}^{\{k'\}}(\text{app})P_{q'\pm}^{\{k'\}}(\beta_a)}{P_{q+}^{\{k\}}(\beta_a)}\right), \tag{21a}$$

where

$$(k,q)=(1,0+);\quad (k',q')=(2,2-) \quad \text{(case I)}, \tag{21b}$$

$$(k,q)=(1,1+);\quad (k',q')=(2,1-) \quad \text{(case II)}. \tag{21c}$$

Normally, the experimentalist would choose to carry out the experiment with left and right circularly polarized light ($\beta=\pm 45°$) if $A_{q'\pm}^{\{k'\}}$ is zero or has been measured. Alternatively, one can perform the experiment at the ellipticities for which $P_{q'\pm}^{\{k'\}}(\beta_a)$ is zero. Some fast polarization switches (such as photoelastic modulators) allow measurements at any ellipticity, not just with circularly polarized light. In fact, for meaningful error analysis, the measurement of orientation should be performed with several pairs of ellipticities. Note that for LIF with spatially resolved detection, the degree of circular polarization, $C=[I(+\beta_a)-I(-\beta_a)]/[I(+\beta_a)+I(-\beta_a)]$, reported alone, is of limited meaning because it does not account for the fact that the line strength depends on J_i and J_e nor does it correct for the alignment. However, by substituting the degree of circular polarization, $C(J_i,J_e)$, for the first term in Eq. (21a) and setting $\beta_a=45°$, we can convert the information in the degree of circular polarization into the expectation value of angular momentum operators:

$$A_{q\pm}^{\{k\}}(J_i,J_e)(\text{app})=C(J_i,J_e)\cdot[P_{0+}^{\{0\}}(J_i,J_e,\beta_a=45°)/P_{q\pm}^{\{k\}}(J_i,J_e,\beta_a=45°)], \tag{22}$$

where $(k,q)=(1,0+)$ and $A_{2-}^{\{2\}}(\text{app})=0$ for case I and $(k,q)=(1,1+)$ and $A_{1-}^{\{2\}}(\text{app})=0$ for case II.

ACKNOWLEDGMENTS

We would like to thank E. Hasselbrink, D. J. Rakestraw, and R. Zhang for many useful discussions. The computations were performed at the Stanford Cell Biology Computer Center under N.S.F. DMB 84-00396 with the assistance of B. Hurja. We would also like to acknowledge the assistance of J. Choi in preparing the figures. This project was supported by the Office of Naval Research under N00014-87-K-0265.

[1] A. C. Kummel, G. O. Sitz, and R. N. Zare, J. Chem. Phys. **85**, 6875 (1986).
[2] A. C. Kummel, G. O. Sitz, and R. N. Zare, J. Chem. Phys. (to be published).
[3] D. A. Case, G. M. McClelland, and D. R. Herschbach, Mol. Phys. **35**, 541 (1978).
[4] C. H. Green and R. N. Zare, J. Chem. Phys. **78**, 6741 (1983).
[5] R. N. Dixon, J. Chem. Phys. **85**, 1866 (1986).
[6] A. J. Bain and A. J. McCaffery, J. Chem. Phys. **83**, 2627 (1985).
[7] I. V. Hertel and W. Stoll, Adv. At. Mol. Phys. **13**, 113 (1978).
[8] G. E. Hall, N. Sivakumar, P. L. Houston, and I. Burak, Phys. Rev. Lett. **56**, 1671 (1986).
[9] G. Herzberg, *Spectra of Diatomic Molecules* (Van Nostrand Reinhold, New York, 1950).
[10] R. N. Zare, A. L. Schmeltekopf, W. J. Harrop, and D. L. Albritton, J. Mol. Spectrosc. **46**, 37 (1973); R. N. Zare, *Molecular Spectroscopy: Modern Research*, edited by K. N. Rao and C. W. Mathews (Academic, New York, 1972), pp. 207–221.
[11] L. T. Earls, Phys. Rev. **48**, 423 (1935).
[12] E. Hill and J. H. Van Vleck, Phys. Rev. **32**, 250 (1928).
[13] J. A. Guest, M. A. O'Halloran, and R. N. Zare, Chem. Phys. Lett. **103**, 261 (1984).